ADVANCING

MICROELECTRONICS

EVERYTHING IN ELECTRONICS BETWEEN THE CHIP AND THE SYSTEM!

MARCH/APRIL 2020
Vol. 47 No. 2

Medical Electronics

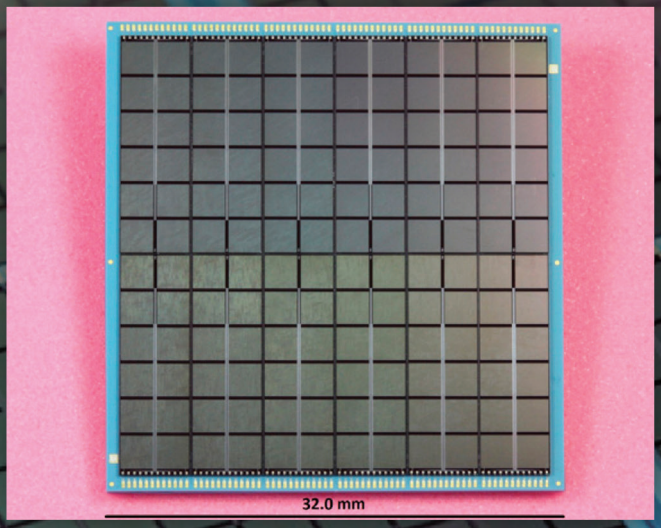

INSIDE THIS ISSUE

iMAPS®

WWW.IMAPS.ORG

LTCC-Based Highly Integrated SiPM Module with Integrated Liquid Cooling Channels for High Resolution Molecular Imaging

Rainer Dohle,[1] Ilaria Sacco,[2,3] Thomas Rittweg,[1] Thomas Friedrich,[1] Gerold Henning,[1] Jörg Goßler,[1] and Peter Fischer[2]*

Abstract

We present a very compact hybrid detection module based on an advanced liquid-cooled low temperature cofired ceramic (LTCC) substrate. The double sided hybrid combines 144 photo detectors and four specialized flip chip readout ASICs (Application Specific Integrated Circuits) used for the readout of scintillation crystals with application in time-of-flight positron emission tomography (PET) combined with magnetic resonance imaging (MRI). If MRI images and PET images are combined, completely new medical diagnostic and treatment prospects are feasible because the two techniques are complementary and they will offer both anatomical and functional information. One of the biggest challenges is the development of miniaturized detector modules that are highly functional and MRI compatible. Our SiPM (Silicon Photomultiplier) module has an area of 32.8 by 32.0 mm2 and contains 12 x12 SiPMs in a pitch of 2.5 mm2. The SiPM readout of the 144 channels is performed by four PETA6 ASICs. The LTCC substrate with a 2.1 mm thickness has been manufactured using the most advanced technologies developed at Micro Systems Engineering GmbH. To guarantee the manufacturability in serial or mass production, DP951 P2 green tape has been used. For the cooling channels, special technology has been developed by MSE. The liquid cooling channels inside the LTCC substrate provide excellent cooling for the ASICs, the SiPMs, and thermal insulation between ASICs and SiPMs and allow a very compact design of the detector modules, reducing their height by 50% compared with other technical solutions. We can insert a ring of our modules in an existing MR (Magnetic Resonance) scanner. Operating the SiPMs at low temperature improves their performance, reducing the effects of dark count rate and improving image quality. There is no heatsink, heat pipe, or other cooling element attached to the back side of the ASICs. To avoid interference between the PET and MRI system, short signal length is required for minimizing pickup loops and eddy currents. The 12 SiPM arrays with 2x6 geometry are wire bonded only at the edges of the SiPMs to the LTCC, enabling the use of nearly the whole detector area for photon detection, which is of paramount importance for excellent image quality. At the opposite side of the substrate, four ASICs with 272 µm bump pitch are flip chip solder assembled to the LTCC substrate including underfilling, and a few SMD (Surface Mount Device) components are mounted. A scintillator crystal array on top of the SiPMs converts gamma rays (511 keV photons produced from positron-electron annihilation) into light. We assume that the LTCC substrates and all components are fully MRI compatible, which is important for the integration of PET with MRI without mutual interference. The paper elucidates the impact of the used technology on the performance of advanced PET/MRI detector modules.

Key words
LTCC, liquid cooling, thermal management, PET/MRI, SiPM

[1] Micro Systems Engineering GmbH, Schlegelweg 17, Berg/Oberfranken 95180, Bavaria, Germany
[2] Lehrstuhl für Schaltungstechnik und Simulation, Institut für Technische Informatik der Universität Heidelberg, B6, 26, Mannheim 68131, Germany
[3] School of Medicine, Radiology Department, Stanford University, Stanford, California 94305-5128
*Corresponding author; email: rainer.dohle@mst.com

INTRODUCTION

Molecular Imaging emerged in the early 21st century as a discipline at the intersection of molecular biology andin vivo imaging. It enables the visualization of cellular functions and the following of molecular processes in living organisms without perturbing them. Molecular imaging differs from traditional medical imaging in that probes known as biomarkers are used to help image particular targets or pathways. We present the technology for high-density gamma ray detector modules for positron emission tomography (PET)/magnetic resonance tomography (MRT) applications. This technique combines a magnetic resonance imaging (MRI) scanner and fully integrated PET detectors allowing for the simultaneous acquisition of PET data during the application of regular MRI techniques. PET imaging is based on detecting two time-coincident high-energy photons generated from the annihilation of an electron with a positron. By imaging the distribution of this positron emitter tracer, it is possible to noninvasively obtain information about molecular processes inside the human body. If the particle arrival time **t** in the detector is measured with sufficiently high precision, it is possible to localize the annihilation event along the line of flight, see Fig. 1. Each square represents a portion of space in the scanner field of view, and its intensity of color is the probability that the event has been originated in that portion of space (the 3-D pixel is called "voxel"). Darker red color corresponds to higher probability.

If time-of-flight (TOF) is not available, all voxels on the line of response have the same probability to contain the annihilation event. When TOF is available, the time information can be used to estimate the original position of the annihilation event. In Fig. 1, t_1 is the time required for the gamma particle for traveling from the annihilation point to the first detector, and t_2 is the time required for the gamma particle for traveling from the annihilation point to the second detector. If the time measurement is precise enough, the annihilation point, which is at a distance D from the ring center of the scanner along the line of response, can be measured as

$$D=(t_1-t_2)\times c=2; \qquad (1)$$

where c is the speed of light. The probability distribution of the annihilation position along the line of response in this case is a Gaussian distribution around the center point of *D*, and its full-width-at-half-maximum (FWHM) is the coincidence time resolution (CTR). CTR is used to express the ability of the system to distinguish two events that happen close in space, where lower values correspond to a better image resolution. A more detailed description of the physics behind PET imaging and TOF can be found in [1-3]. MRI is a medical imaging technique used to investigate the anatomy and physiology of the body. The physics of this technique involves the interaction of matter with electromagnetic fields. MRI provides an excellent soft-tissue contrast [1]. The major challenge in combining PET and MRI is establishing mutual compatibility. Many new applications for combined PET/MRI are beginning to emerge.

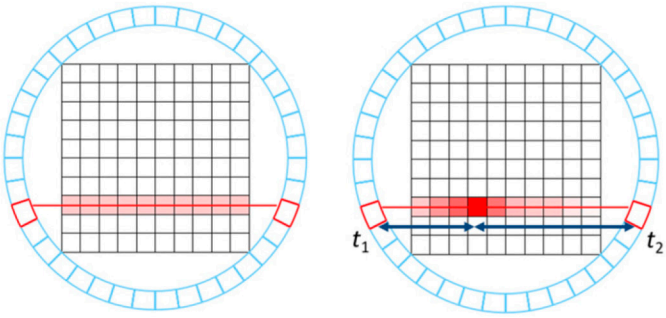

Fig. 1. Principle of TOF: left side without TOF, the annihilation position probability is uniform for all voxels along the line of response (red). Right side with TOF, the probability distribution is a Gaussian distribution along the line of response; the width depends on the time resolution.

These applications presuppose improved image quality, shorter scanning times, reduced radiation dose (especially important for pediatric imaging), and more precise quantification. Our detector modules are designed for clinical whole body applications and to be integrated into a 3T, 5T, or even 7T MRT, but can be adapted for preclinical applications. The central gamma detection elements in the PET/MR (Magnetic Resonance) scanners are "detector cubes" which contain the scintillator crystals, SiPMs, and readout electronics. They also contain special cooling units that dissipate the heat generated in the sensors and electronics, and keep the photo detectors at low temperature for a reduction of the dark count rate.

The form factor of the detector modules is very important because the maximum height of the PET modules is determined by the space constraints imposed by the surrounding MR scanner.

A. Comparison with the State of the Art

Currently commercially available TOF PET/CT (Computed Tomography) and PET/MRI scanners have a CTR higher than 300 ps FWHM [4-6] and a larger form factor. A simultaneous detection is termed a "coincidence."

For illustration and comparison, Fig. 2 shows a cube with 64 channels as it had been developed in the HYPER-Image project [6] (left) and a SUBLIMA (SUB nanosecond Leverage In PET/MR ImAging) cube (right), which despite the much larger number of channels, is more compact and has much better performance (see Electrical performance section).

B. Improvements of Our Solution

The performance of the individual components (SiPMs and ASICs) has been significantly improved and their properties are now beyond state of the art. The time resolutions obtained in various setups have increased by more than a factor of two and are among the best available today, particularly on a system level.

One big advantage of the detector modules (Fig. 3) developed within the SUBLIMA project [7] is the lower

continued on page 12

continued from page 11

height of the modules (Fig. 2), enabling larger rings or a smaller size of the PET/MRT scanners.

C. Scope and Content of This Paper

The scope of this paper is the design of the low temperature cofired ceramic (LTCC) substrates and the detector modules as well as the used technologies.

The Detector module design section outlines the detector module design. The manufacturing technology section describes the manufacturing technologies used to build the modules. The Results section shows a few selected measurement highlights, especially those connected to the improvements possible because of liquid cooling. The Discussion section gives a short discussion of our work and the Conclusion section summarizes our conclusions. The Outlook section shows future work and applications.

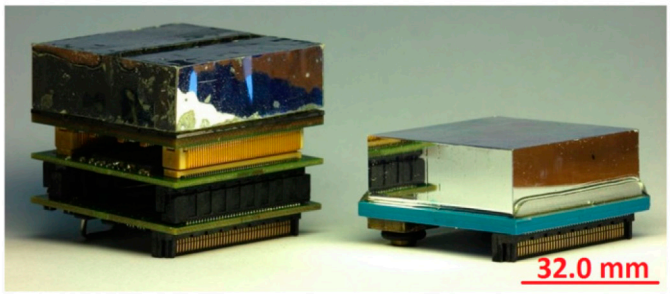

Fig. 2. Detector modules with wrapped scintillator crystal arrays. The left cube was the outcome of the HYPERImage project [6]; the right cube shows one of the SUBLIMA results (having twice as many channels and a much lower height). The liquid-cooled SUBLIMA modules are advantageous when size and performance are of paramount importance.

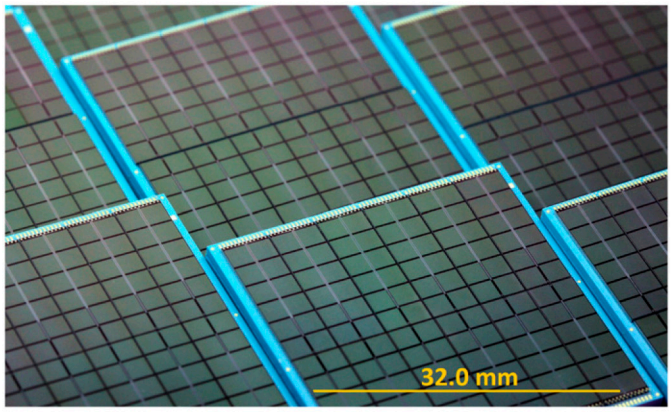

Fig. 3. Modules with SiPMs manufactured at MSE.

Fig. 4. Cross section of the sintered substrate (dimensions 32.8 by 2.2 mm; without components) showing the LTCC layer stack with the cooling channels and the vias.

SiPM technologies and scintillator engineering are likewise important, but are outside of the scope of this paper. A pool of available information can be found in the cited literature.

DETECTOR MODULE DESIGN

A. Low Temperature Cofired Ceramic Design

The LTCC substrate has been designed in close cooperation with Heidelberg University.

The following design rules have been used:

1. Via diameter: 100 µm
2. Catch pads inner layer: 150 µm
3. Catch pads outer layer: 200 µm
4. Hatch: Lines/Spaces: 150 µm/362 µm
5. Routing: Lines/Spaces: ≥100 µm/≥150 µm
6. Flip Chip Pitch: 272 × 272 µm²

Fig. 4 shows a cross section of the LTCC substrate.

The 2.2 mm thick LTCC substrate is fully MRT compatible, i.e., it will not disturb the magnetic field nor impair image quality. Hatched planes prevent eddy currents.

B. Hybrid Circuit Design

The bottom side of the LTCC substrate is populated with four PETA6 flip chips, one small form-factor connector, and only a few SMD components. The used PETA6 flip chips have been designed for high data rate operation. Compared with the PETA5 ASICs, used in [8], they have new features and much higher performance, summarized in Table I [9].

The chip includes 36 channels, available with both single-ended and differential-ended front-end. The power consumption has been reduced compared with the previous chip version and the readout frequency has been doubled. Additional features for applications at a high data rate have been included, such as zero suppression readout, an internal buffer for one event data storing, and additional low voltage differential signal (LVDS) output lines. The integrated time to digital converter assigns time-stamp information per radiation event with a bin width of 50 ps [9]. This technology is compatible with any SiPM available on the market [9]. A floating diode has been integrated and can be used for temperature measurements.

Liquid cooling solution is one of the most effective techniques for thermal management [10, 11]. Inlet and outlet for the cooling liquid can be soldered and/or glued onto the substrate. Please note that there is no heatsink or other cooling element attached to the back side of the chips, see Figs. 5 and 6. The cooling of the ASICs relies only on the cooling channels located inside of the LTCC. This reduces not only the junction temperature of the ASICs but also provides a nearly perfect thermal isolation between the bottom side and the top side of the LTCC, which is a big advantage compared with the use of a traditional PCB (Printed Circuit Board) and a traditional thermal management heatsink.

One PETA6 chip generates about 1.2 W of heat at optimal performance (one PETA5 chip generates about 1.6 W at optimal performance). The peak power density is about 4 W/cm² for PETA6 chips (and about 5.3 W/cm² for PETA5 chips). Channel dimensions and flow rate were selected experimentally.

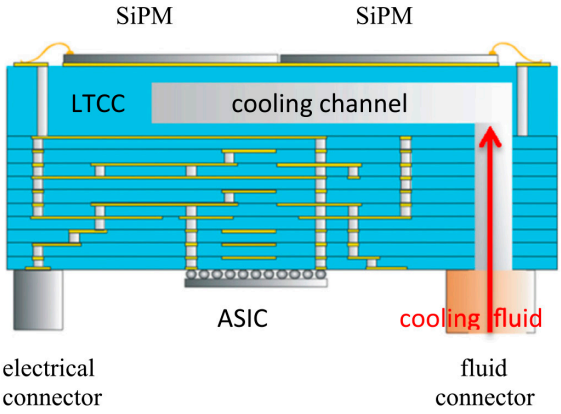

Fig. 5. Schematic cross section (not to scale) of the liquid-cooled SiPM module showing the LTCC layer stack with the cooling channel, the electrical connector (left), and the water connector (right).

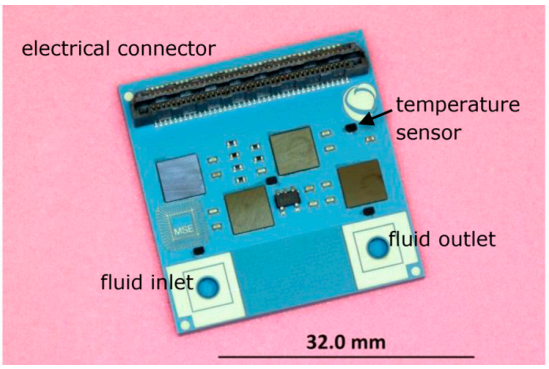

Fig. 6. Module with four PETA6 ASICS and SMDs.

We assume that all components are MRI compatible, i.e., they will not derange the magnetic field nor deteriorate image quality. Experiments on the system level are ongoing.

At the opposite side of the substrate shown at Fig. 6/ Fig. 7 are 12 SiPM tiles very closely arranged to each other (Fig. 8) to maximize the light collection from scintillating crystals. This complements the high fill factor of the SiPM tiles.

The SiPMs are wire bonded to the LTCC substrate at two opposite edges of the substrate, see Figs. 8 and 9. Our design maximizes the active area (e.g., has minimal "dead space" outside of the active area) and therefore minimizes the loss of photons (without the requirement to have through-silicon vias [TSVs] in the SiPMs). The obtained higher fill-factor will be conducive to a higher quality reconstructed medical image.

Our LTCC and assembly technologies will allow the use of SiPMs with TSVs [12] as well.

It should be noted that the SiPMs produce heat as well (on the order of a few mW in each tile). In comparison with the ASICs, this amount of heat is negligible, however. This allows the use of a conductive adhesive for the connection between SiPMs and LTCCs. Silver sintering or the use of a solder is not necessary at this

Table I
Features and Performance of PETA5/PETA6

Features and performance	PETA5	PETA6
Power consumption (mW/channel)	43	33
Single ended polarity	Negative	Negative/positive
Readout frequency (MHz)	160	311
Bypass readout	No	Yes
Channel data (bit)	37	34
LVDS outputs	2	2 (+2)
Double buffer	No	Yes
Integrated temperature sensor	No	Yes

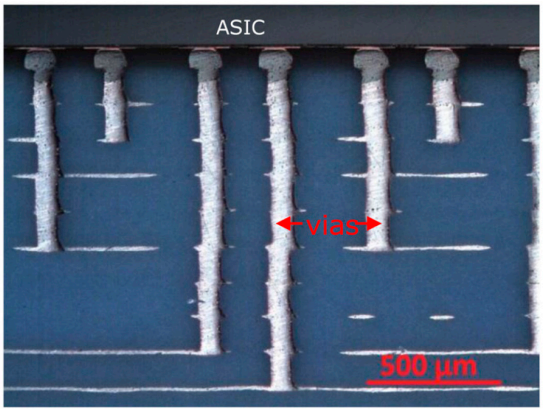

Fig. 7 Cross section with PETA6 ASIC and LTCC (detail).

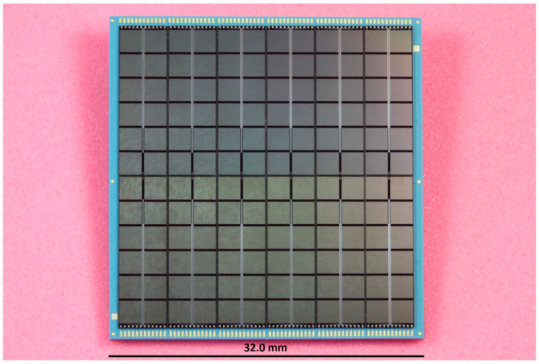

Fig. 8. PETA6 module with 12 rectangular SiPM tiles. Each SiPM die contains 12 sensors.

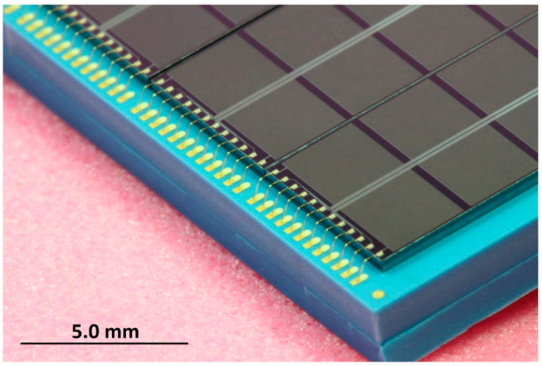

Fig. 9. Detailed view showing the gold wire bonds.

continued on page 14

continued from page 13

interface because the SiPMs do not produce a lot of heat during operation as outlined previously.

C. Design of the Detector Cubes

On top of the 12 SiPM tiles resides a scintillator crystal array (Fig. 10) made from lutetium-yttrium oxyorthosilicate (LYSO). The scintillators convert the received gamma rays into light with a wavelength (λ = 420 nm) suitable to be detected by the SiPMs.

MANUFACTURING TECHNOLOGY

A. Low Temperature Cofired Ceramic Manufacturing

The LTCC substrate has been built with DP951 P2 green tape. Three layers contain the cooling channel. The channel has been laser structured. The sintered width of this channel is 2.6 mm; the height is approximately 0.4 mm. The access holes to the cooling channel and the vias are mechanically punched. The LTCC substrate manufacturing yield was 71.43%. It should be noted that there is always a learning curve conducive to higher yield over time.

Fig. 10. Detector cube #2 with scintillator array, ASIC side with coolant connectors.

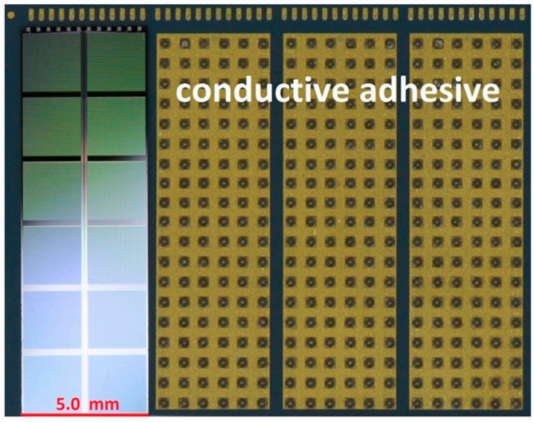

Fig. 11. The SiPMs are mounted with conductive glue (photo from the first experiment).

B. Hybrid Manufacturing

SMD assembly and flip chip assembly were performed in two separate manufacturing steps to reduce the risk, using lead-free solder paste for the nickel-free SMD components. Because the flip chips have lead-free solder bumps, the combination of both manufacturing steps is possible. After reflow soldering, the flip chips were underfilled using a high performance underfill with sufficient thermal conductivity qualified in previous work [13, 14].

The 12 SiPMs have been die bonded to the modules with a Datacon 2200 Evo machine using silver-filled conductive adhesive, printed in a regular pattern (see Fig. 11). Because of the low CTE (Coefficient of Thermal Expansion) mismatch between LTCC and silicon and the low curing temperature, the mechanical stress induced in the SiPM tiles is negligible. After curing, the SiPMs were wedge-wedge wire bonded from the die to the substrate using gold wire with 25 µm diameter. The total yield was 100%.

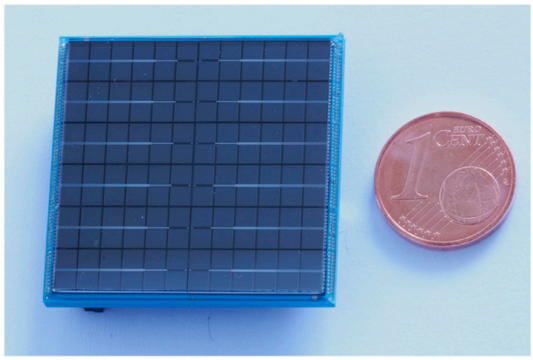

Fig. 12. Detector module with SiPMs before scintillator crystal array mounting.

C. Scintillator Crystal Array Mounting

The detector cube is completed by gluing a scintillator crystal array on top of the SiPMs and by sealing the wire bonds. The scintillator crystal arrays were mounted to the hybrids (Figs. 12 and 13) at Heidelberg University employing a proprietary technology. It should be noted that scintillator crystal properties and scintillator crystal array mounting have a large impact on detector performance.

Scintillator properties and limitations are explained in [15] already. A detailed review of scintillator engineering can be found in [16].

RESULTS

A. Thermal Performance

Compared with air cooled modules, or modules where the ASICs are cooled with water-cooled copper pipes from the back side, we obtained superior results, resulting in a much lower operating temperature of the ASICs as well as the SiPMs. It could be shown, that a completely sufficient cooling with room temperature water is possible. We selected water because of its

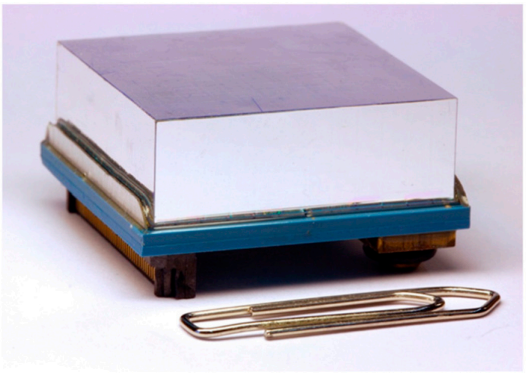

Fig. 13. Detector cube with attached pixilated scintillator array on top.

high specific heat and for the simplicity of the setup. A reduced time to thermal stability of the detector module (10 s) compared with air cooling (130 s) and water cooled copper pipes at the backside of the ASICs (44 s) has been measured [8]. The measurements were taken with a water flow of 0.1 L/min and a water temperature of 21°C at the inlet.

B. Electrical Performance

Many ambitious objectives of the original Description of Work of the SUBLIMA project have even been exceeded [7]. Chip layout and ASIC layout have been carefully studied for avoiding loops in traces, which would cause noise pickup from the MR gradient field. Especially important is the obtained CTR of about 200 ps. This is extremely important for improving image

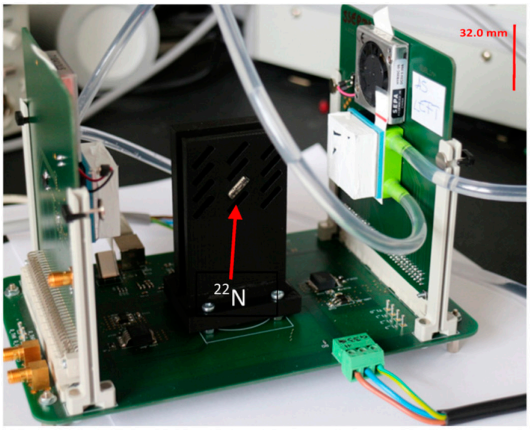

Fig. 14. Measurement setup for the laboratory. Between detector cubes #1 and #2, a positron emitting source such as ^{22}Na has been placed.

resolution. Fig. 14 shows the measurement setup (with positron source) for the laboratory.

Fig. 15 shows the paired CTR obtained with 10 mm long LYSO arrays with 2.25 mm crystal size (2.5 mm pitch) at room temperature and at 34°C (lower temperatures and codoped LYSO scintillator crystal arrays could lead to even lower CTR [17, 18]).

The temperature has been measured with four sensors (shown in Fig. 10) mounted to the LTCC as well as an Infraredcamera. Fig. 15 shows clearly, that a lower temperature of the SiPM tiles improves CTR, i.e., the performance of the PET/MR scanner increases. The operating temperature of the SiPMs can be adjusted to the

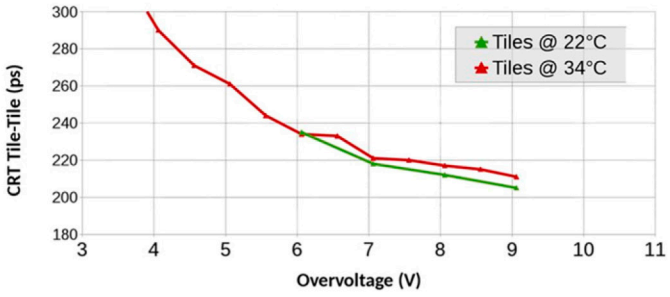

Fig. 15. CTR (FWHM) between two channels on two SiPM tiles at different temperatures (T = 22°C and T = 34°C) in dependence on the overvoltage applied to the SiPMs.

optimal value with the appropriate temperature of the cooling liquid.

Although sub100 ps CTR has been reported in the literature for short scintillator crystals (3 mm length) [17], clinical PET requires scintillation crystals with 10-20 mm length to provide suitable stopping power for 511 keV photons. Increased crystal length reduces the light collection efficiency and increases the scintillation photon transit time variance, resulting in substantial increased CTR [18].

Fig. 16 shows another important improvement of the detector modules with PETA6 ASICs in comparison with detector modules with PETA5 modules (reported in [8]). The hit loss (radiation events that are not detected) percentage depends on the readout frequency, the channel dead time, and the overall hit rate per channel. All these parameters are reported in the following plot. The simulation takes into account only 511 keV events

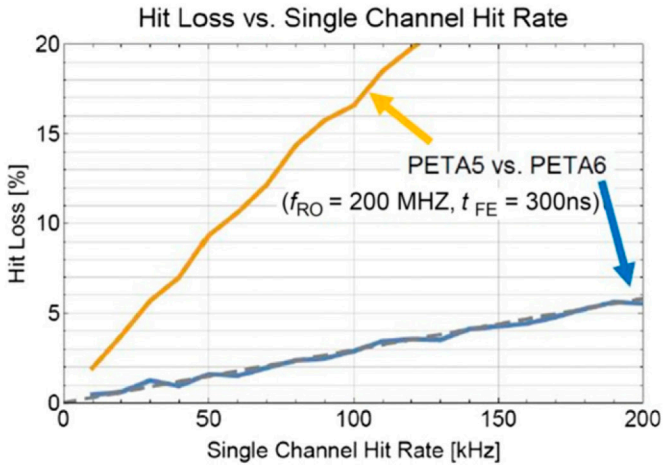

Fig. 16. Hit loss versus single channel hit rate for PETA5 and PETA6 modules (f_{RO} = readout frequency, t_{FE} = dead time of the front-end).

continued on page 16

continued from page 15

assuming operation at room temperature. A lower hit loss improves image quality.

DISCUSSION

A. Size of the Modules

Compared with the HYPERImage modules and other technical solutions [6] we could reduce the height (volume) of the modules by a factor of about two despite largely increased functionality because of abolition of one circuit board. This height reduction is not only important to integrating PET into a MR scanner, it is critical because of the given space limitations inside the scanner. A reduced module height enables larger rings for heavier patients or a smaller size of the PET/MR scanners.

B. Thermal Performance

We could show that the heat generated by the four ASICs can be removed easily without a large increase of the junction temperature. The heat generated by the SiPMs is, as a first approximation, negligible. We obtained a nearly perfect isolation between ASICs and SiPMs and a nearly homogeneous temperature at the top (SiPM) side of the LTCC substrate. Although the temperature dependency of the SiPMs could be reduced by Fondazione Bruno Kessler (FBK) over the time span of the SUBLIMA project [19, 20], a lower operating temperature of the SiPMs and a homogeneous temperature distribution is still advantageous [21]. Because of the high hardness of the LTCC material and the resulting abrasion resistance, we assume a much longer lifetime of the modules as it would be possible using other technical cooling solutions as per description in [22] or [23].

C. Electrical Performance

The advantage of TOF is the improvement in image signal to noise ratio (SNR) [24]. Already, early work has shown that TOF information produces improved images for all patient sizes [25]. According to [18], more than a factor of five improvements in image SNR is possible at 100 ps FWHM CTR compared with non-TOF PET. Based on the analysis found in [26, 27], we can define an improvement factor G as

$$G = SNR_{TOF}/SNR_{Non-TOF} = (2D/c \times \Delta t)^{1/2}; \quad (2)$$

where D is the diameter of the object being imaged, c is the speed of light, and Δt is the time resolution. We did not measure the improvement factor, however. An improved SNR allows for either a reduced scan time [28] or improved image quality of the reconstructed image for the same scan time [26]. Better SNR also means that the examination time and radioactive dose received by the patient [15, 25, 28-34] can be reduced while at the same time improving the detectability of lesions [35-38].

D. Leakage Concerns

Even though the leakage issue might be a concern, we did not observe any leakage in our laboratory setup. The LTCC substrate passed the Helium fine leak test according to MIL-STD 883K, Method 1014. The connection between LTCC and water inlet or water outlet has been soldered and in addition secured with glue. For the implementation of the modules in a PET/MR scanner, we recommend commercial connectors and tubes.

CONCLUSIONS

We have shown that it is possible to reduce the size of SiPM modules for PET/MR applications and increase their electrical performance considerably. The modules are highly advantageous when small size is paramount. There is a growing recognition of the benefits of simultaneous PET/MRI for molecular imaging [34] such as oncology [39], quality assurance in hadron therapy [40], cerebral blood flow [41], cardiac PET/MRI [42], and brain functions [43]. Those systems will be beneficial to pediatric patients in particular, given the large reduction in radiation dose compared with PET/CT [32, 33].

OUTLOOK

Five detector modules will be assembled to a module block (Fig. 17). The final goal is a complete PET ring for a full-body scanner with many module blocks (Fig. 18).

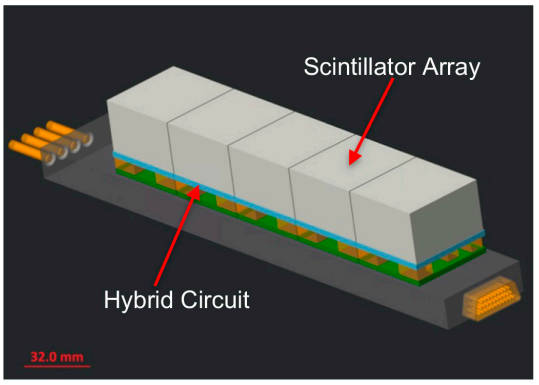

Fig. 17. Module block with five detector modules with an attached pixilated scintillator array on top of each module (schematic view).

A full PET ring using the scintillator configuration described in this work will be intensely studied for TOF performance and MR compatibility. This will allow an evaluation for a clinical scintillator and readout configuration using SiPMs on a full system level. Actuality and importance of the work discussed in this paper have been confirmed in [44]. The developed modules for clinical applications have been adapted for preclinical applications [34]. In addition to molecular imaging [35], those radiation detectors can be used in a large variety of fields [41], including medical dosimetry [37], homeland security, nuclear nonproliferation [38], nondestructive detection, high-energy physics, and gamma ray astronomy.

ACKNOWLEDGMENTS

The authors thank Claudio Piemonte and Nicola Zorzi from FBK for the SiPMs and Elke Beyer, Christian Zeilmann, Henryk Lutsch-Kelemen, and Fabian Rittweg for contribution to and valuable support of this work. We thank Thomas Dünne for taking part of the photos and Bernd Burger for cross-sectioning of samples. Early parts of this work have been supported under

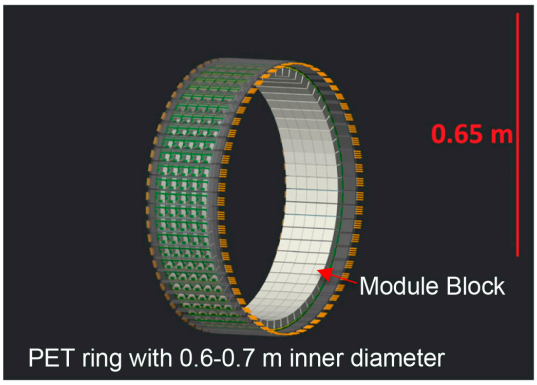

Fig. 18. PET ring for a full-body PET/MR scanner (schematic view).

the HEALTH priority of the European Union's Seventh Framework, project SUBLIMA under grant 241711.

REFERENCES

[1] S.L. Bacharach, "Positron emission tomography," In: V. Dilsizian and G.M. Pohost, eds., *Cardiac CT, PET and MR*, 2nd ed., pp. 3-29, Blackwell, Hoboken, NJ, 2010.

[2] V.C. Spanoudaki and C.S. Levin, "Photo-detectors for time of flight positron emission tomography (ToF-PET)," *Sensors (Basel)*, Vol. 10, pp. 10484-10505, 2010.

[3] R.G. Wells and R.A. deKemp, "Does time-of-flight improve image quality in the heart," *Journal of Nuclear Cardiology*, pp. 1-4, 2017.

[4] M. Miller, J. Zhang, K. Binzel, J. Griesmer, T. Laurence, M. Narayanan, D. Natarajamani, S. Wang, and M. Knopp, "Characterization of the vereos digital photon counting PET system," *Journal of Nuclear Medicine*, Vol. 56, p. 434, 2015.

[5] C.S. Levin, S.H. Maramraju, M.M. Khalighi, T.W. Deller, G. Delso, and F. Jansen, "Design features and mutual compatibility studies of the time-of-flight PET capable GE SIGNA PET/MR system," *IEEE Transactions on Medical Imaging*, Vol. 35, No. 8, pp. 1907-1914, 2016.

[6] P. Fischer and M. Ritzert, "Final report HYPERImage," Heidelberg University, 2011.

[7] P. Fischer, I. Sacco, R. Dohle, M. Ritzert, and C. Piemonte, "Final report SUBLIMA, WP3—PET/MR detector cubes," March 2015. http://www. sublima-pet-mr.eu

[8] R. Dohle, T. Rittweg, V. Chernyshev, E. Beyer, J. Goßler, I. Sacco, and P. Fischer, "Very compact, water-cooled SiPM module for PET/MRT applications," Proceedings EMPC, Friedrichshafen, Germany, September 14-16, 2015.

[9] I. Sacco, "Development of highly integrated PET/MR detector modules," Ph.D. dissertation, Heidelberg University, Heidelberg, November 9, 2016.

[10] Y. Mizuno, I. Soga, S. Hirose, O. Tsuboi, and T. Iwai, "Si microchannel cooler integrated with high power amplifiers for base station of mobile communication systems," Proceedings 61st ECTC, Lake Buena Vista, FL, pp. 1541-1546, May 31-June 3, 2011.

[11] E.G. Colgan, B. Furman, M. Gaynes, W. Graham, N. LaBianca, J.H. Magerlein, R.J. Polastre, M.B. Rothwell, R.J. Bezama, R. Choudhary, K. Marston, H. Toy, J. Wakil, J. Zitz, and R. Schmidt, "A practical implementation of silicon microchannel coolers for high power chips," *IEEE Transactions on Components and Packaging Technologies*, Vol. 30, No. 2, pp. 218-225, 2007.

[12] A. Ferri, F. Acerbi, A. Gola, D. Krabe, T. Lichtenegger, G. Paternoster, C. Piemonte, and M. Stich, "High density interconnect NUV-HD SiPMs: performance assessment (#3284)," IEEE Nuclear Science Symposium & Medical Imaging Conference, MIC Poster Session III, M-15, Atlanta, GA, October 27, 2017.

[13] R. Dohle, F. Schüßler, J. Goßler, T. Oppert, and J. Franke, "Adapted assembly processes for flip-chip technology with solder bumps of 50 µm or 40 µm diameter," 3rd Electronic Systems-Integration Technology Conference, Berlin, Germany, September 13-16, 2010.

[14] R. Dohle, S. Härter, J. Goßler, and J. Franke, "Accelerated life tests of flip- chips with solder balls down to 30 µm diameter," 44th International Symposium on Microelectronics, Long Beach, California, October 9-13, 2011.

[15] P. Lecoq, "Development of new scintillators for medical applications," *Nuclear Instruments and Methods in Physics Research A*, Vol. 809, pp. 130-139, 2016.

[16] M. Nikl and A. Yoshikawa, "Recent R&D trends in inorganic single- crystal scintillator materials for radiation detection," *Advanced Optical Materials*, Vol. 3, No. 4, pp. 463-481, 2015.

[17] M.V. Nemallapudi, S. Gundacker, P. Lecoq, E. Auffray, A. Ferri, A. Gola, and C. Piemonte, "Sub-100 ps coincidence time resolution for positron emission tomography with LSO:Ce codoped with Ca," *Physics in Medicine and Biology*, Vol. 60, pp. 4635-4649, 2015.

[18] J. Cates and C.S. Levin, "Realizing PET systems with 100 ps FWHM coincidence timing resolution," SPIE Optical Engineering and Applications, Proceedings of SPIE Volume 9969, Radiation Detectors, Systems and Applications XVII, San Diego, California, United States, August 28- September 1, 2016.

[19] C. Piemonte, A. Ferri, A. Gola, T. Pro, N. Serra, A. Tarolli, and N. Zorzi, "Characterization of the first FBK high-density cell silicon photomultiplier technology," *IEEE Transactions on Electron Devices*, Vol. 60, No. 8, pp. 2567-2573, 2013.

[20] M. Grodzicka, M. Moszyński, T. Szczęśniak, A. Ferri, C. Piemonte, M. Szawłowski, A. Gola, K. Grodzicki, and A. Tarolli, "Performance of FBK high-density SiPMs in scintillation spectrometry," *Journal of Instrumentation*, Vol. 9, pp. 1-18, 2014.

[21] S. Piatek, "Effects of temperature on the performance of a silicon photomultiplier (SiPM)," [Online]. http://www.hamamatsu.com/eu/en/community/optical_sensors/articles/temperature_and_sipm_performance/index.html, January 2017.

[22] Y. Han, B.L. Lau, X. Zhang, Y.C. Leong, and K.F. Choo, "Enhancement of hotspot cooling with diamond heat spreader on Cu microchannel heat sink for GaN on Si device," *IEEE Transactions on Components, Packaging, and Manufacturing Technology*, Vol. 4, No. 6, pp. 983-990, 2014.

[23] T.E. Sarvey, Y. Zhang, C. Cheung, R. Gutala, A. Rahman, A. Dasu, and M.S. Bakir, "Monolithic integration of a micropinfin heat sink in a 28-nm FPGA," *IEEE Transactions on Components, Packaging, and Manufacturing Technology*, Vol. 7, No. 10, pp. 1617-1624, 2017.

[24] M. Conti, "Focus on time-of-flight PET: the benefits of improved time resolution," *European Journal of Nuclear Medicine and Molecular Imaging*, Vol. 38, No. 6, pp. 1147-1157, 2011.

[25] J. Karp, S. Surti, M. Daube-Witherspoon, and G. Muehllehner, "Benefit of time-of-flight in PET: experimental and clinical results," *Journal of Nuclear Medicine*, No. 49, p. 462f, 2008.

[26] W.W. Moses, "Time of flight in PET revisited," *IEEE Transactions on Nuclear Science*, Vol. 50, No. 5, pp. 1325-1330, 2003.

[27] S. Surti, J. Karp, L. Popescu, M. Daube-Witherspoon, and M. Werner, "Investigation of time-of-flight benefit 3-D PET," *IEEE Transactions on Medical Imaging*, Vol. 25, No. 5, pp. 529-538, 2006.

[28] I.S. Armstrong, C.M. Tonge, and P. Arumugam, "Assessing time-of-flight signal-to-noise ratio gains within the myocardium and subsequent reductions in administered activity in cardiac PET studies," *Journal of Nuclear Cardiology*, pp. 1-8, 2017.

[29] R. Fazel, H.M. Krumholz, Y. Wang, J.S. Ross, J. Chen, H.H. Ting, N.D. Shah, K. Nasir, A.J. Einstein, and B.K. Nallamothu, "Exposure to low-dose ionizing radiation from medical imaging procedures," *The New England Journal of Medicine*, Vol. 361, pp. 849-857, 2009.

[30] M.A. Queiroz, G. Delso, S. Wollenweber, T. Deller, K. Zeimpekis, M. Huellner, F. de Galiza Barbosa, G. von Schulthess, and P. Veit-Haibach, "Dose optimization in TOF-PET/MR compared to TOF-PET/CT," *PLoS One*, Vol. 10, No. 7, pp. e0128842, 2015.

[31] S. Gaditis and B. Bender, M. Reimold, and J.F. Schäfer, "PET/MRI in children," *European Journal of Radiology*, 2017.

[32] I.R. Bielsa, "Pediatric nuclear medicine and its development as a specialty," *Seminars in Nuclear Medicine*, Vol. 47, No. 2, pp. 102-109, 2017.

[33] I. Sacco, R. Dohle, P. Fischer, A. Gola, C. Piemonte, and M. Ritzert, "A sub-millimeter resolution detector module for small-animal PET applications," *Journal of Instrumentation : An IOP and SISSA Journal*, Vol. 12, No. 1, C01006, 2017.

[34] S. Abbaszadeh and C.S. Levin, "New-generation small animal positron emission tomography system for molecular imaging," *Journal of Medical Imaging (Bellingham, Wash.)*, Vol. 4, No. 1, p. 011008, 2017.

continued on page 18

continued from page 17

[35] G. El Fakhri, S. Surti, C.M. Trott, J. Scheuermann, and J.S. Karp, "Improvement in lesion detection with whole-body oncologic time-of-flight PET," *Journal of Nuclear Medicine*, Vol. 52, No. 3, pp. 347-353, 2011.
[36] I. Rausch, H.H. Quick, J. Cal-Conzalez, B. Sattler, R. Boellard, and T. Beyer, "Technical and instrumentational foundations of PET/MRI," *European Journal of Radiology*, Vol. 94, pp. A3-A13, 2017.
[37] M. Meshkian, C. Allwork, U. Gendotti, M. Ellis, and P. Schotanus, "Applications of innovative SiPM-based PVT scintillator detectors," Nuclear Science Symposium, session "Instrumentation for Homeland and National Security," Atlanta, Georgia, October 23, 2017.
[38] F. Acerbi, A. Gola, V.V. Regazzoni, G. Paternoster, G. Borghi, C. Piemonte, and N. Zorzi, "Ultra-high cell density silicon photomultipliers with high detection efficiency," Proceedings SPIE #2959, Advanced Photon Counting Techniques XI, Vol. 10212, May 1, 2017.
[39] H. Sotoudeh, A. Sharma, K.J. Fowler, and J. McConathy, "Clinical application of PET/MRI in oncology," *Journal of Magnetic Resonance Imaging*, Vol. 44, No. 2, pp. 265-276, 2016.
[40] A. Del Guerra, N. Belcari, and M. Bisogni, "Positron emission tomography," *Rivista del Nuovo Cimento*, Vol. 39, No. 4, pp. 156-182, 2016.
[41] M.M. Khalighi, T.W. Deller, A.P. Fan, P.K. Gulaka, B. Shen, P. Singh, J.H. Park, F.T. Chin, and G. Zaharchuk, "Image-derived input function estimation on a TOF-enabled PET/MR for cerebral blood flow mapping," *Journal of Cerebral Blood Flow and Metabolism*, Vol. 38, pp. 126-135, 2017.
[42] A. Masuda and Y. Takeishi, "Current status and future direction of PET/MR in cardiology," *Annals of Nuclear Cardiology*, Vol. 3, No. 1, pp. 73-79, 2017.
[43] I. Sacco, C.-M. Chang, B. Lee, M. Ritzert, P. Fischer, and C. S. Levin, "An integrated circuit read-out for TOF-PET detectors for PET/MRI," Proceedings SPIE 10393, Radiation Detectors in Medicine, Industry, and National Security, San Diego, California, United States, September 19, 2017.
[44] S. Chandra and F. Peechta, "Medical imaging and diagnostics: current status and future trends," Keynote Presentation at IMAPS Advanced Technology Workshop on Advanced Packaging for Medical Microelectronics, San Diego, CA, January 23, 2018.